ORIGINAL ARTICLE

Synthesis of 3,3′-methylenebis(4-hydroxyquinolin-2(1H)-ones) of prospective anti-COVID-19 drugs

Ashraf A. Aly[1] · Alaa A. Hassan[1] · Asmaa H. Mohamed[1] · Esraa M. Osman[1] · Stefan Bräse[2,3] · Martin Nieger[4] · Mahmoud A. A. Ibrahim[1] · Sara M. Mostafa[1]

Abstract

During formylation of 2-quinolones by DMF/Et$_3$N mixture, the unexpected 3,3′-methylenebis(4-hydroxyquinolin-2(1H)-ones) were formed. The discussed mechanism was proved as due to the formation of 4-formyl-2-quinolone as intermediate. Reaction of the latter compound with the parent quinolone under the same reaction condition gave also the same product. The structure of the obtained products was elucidated via NMR, IR and mass spectra. X-ray structure analysis proved the *anti*-form of the obtained compounds, which were stabilized by the formation hydrogen bond. Molecular docking calculations showed that most of the synthesized compounds possessed good binding affinity to the SARS-CoV-2 main protease (M^{pro}) in comparable to Darunavir.

Graphic abstract
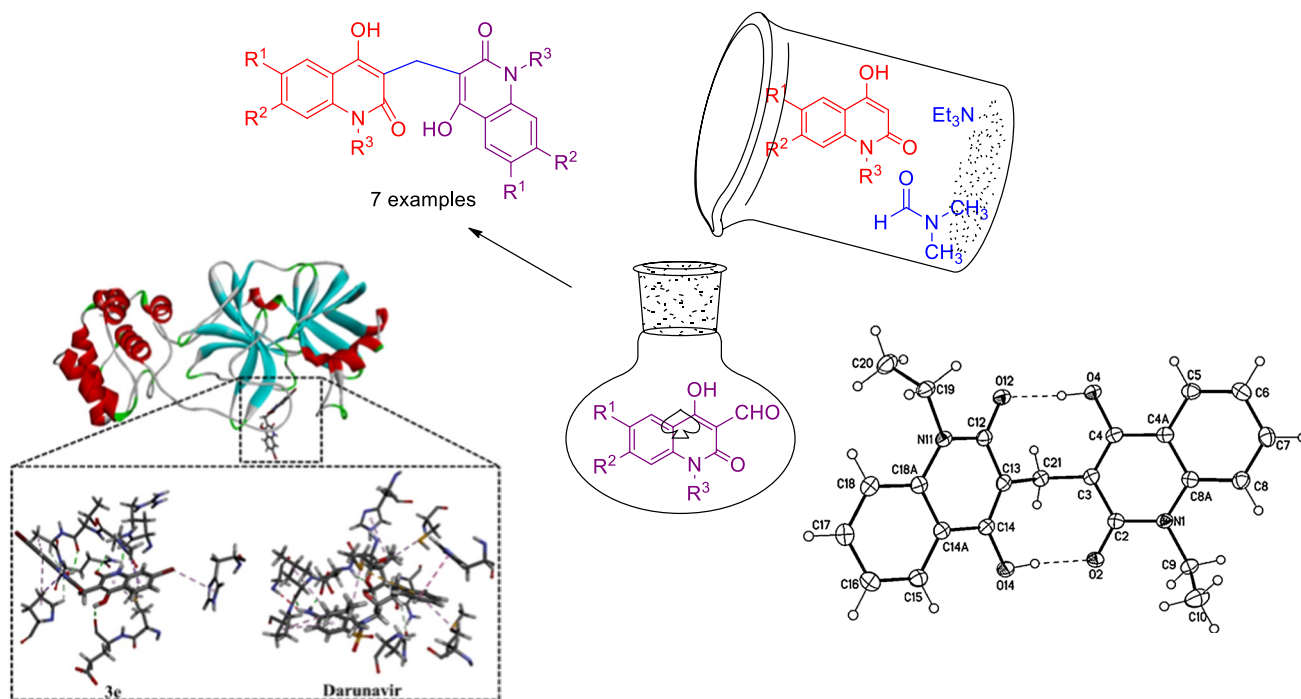
Extended author information available on the last page of the article

Introduction

Dimethylformamide (DMF) can react as either an electrophilic and/or a nucleophilic agent. Therefore, DMF can be considered as the source of various key intermediates mediating a plethora of important reactions [1]. More significantly, DMF can participate in many reactions by serving as a multipurpose building block for various units, such as CH$_3$, N(CH$_3$)$_2$, HCO$_2$, CHO, O, H$^-$, H., (CH$_3$)$_2$CO, etc. (Fig. 1).

Alkyl-quinolones AQ analogs (Fig. 2) act synergistically to inhibit bacterial growth [2, 3] (i.e., two examples assigned as HHQ and HQNP).

Quinolones show a significant similarity to some anticancer [4], anticonvulsant [5–7], anti-dermatities [8], antibacterial [9], antimicrobial [10], anti-Alzheimer [11] and pain relief [12] in addition to their medical, agricultural and industrial uses [13–15]. In previous work with quinolones, Aly et al., synthesized various classes of 2-quinolones such as 2′-amino-2,5′-dioxo-5′,6′-dihydro-spiro(indoline-3,4′-pyrano[3,2-*c*]quinoline)-3′-carbonitriles [16], 3-(methyl-thio)-4-oxo-4,5-dihydrofuro[3,2-c]quinolone-2-carbonitriles [17], 3-(methylthio)-4-oxo-4,5-dihydro-furo[3,2-*c*]quinolone-2-carboxamides [17], naphtho[2′,3′:4,5]furo[3,2-c]quinoline-6,7,12(5*H*)-trione derivatives (as ERK inhibitors with efficacy in BRAF-mutant Melanoma) [18], 2,3-bis-(4-hydroxy-2-oxo-1,2-dihydroquinolin-3-yl)succinates, arylmethylene-bis-3,3′-quinoline-2-ones [19], *N*-2,3-bis(6-substituted-4-hydroxy-2-oxo-1,2-dihydroquinolin-3-yl) naphthalene-1,4-diones and substituted *N*-(methyl/ethyl) bisquinolinone triethylammonium salts [20].

Han and Zhou [21] reported that the reaction of two equivalents of quinolone derivatives with one equivalent of aromatic aldehydes and potassium phtalamide under reflux at water–ethanol solution, gave the corresponding
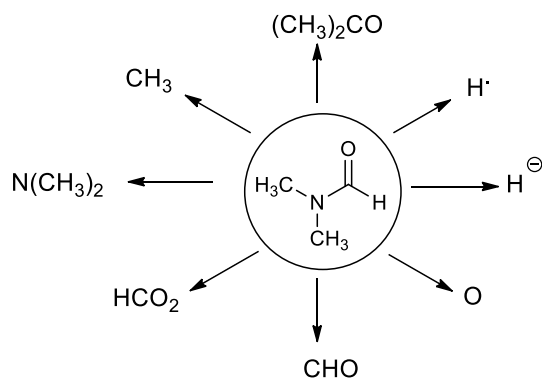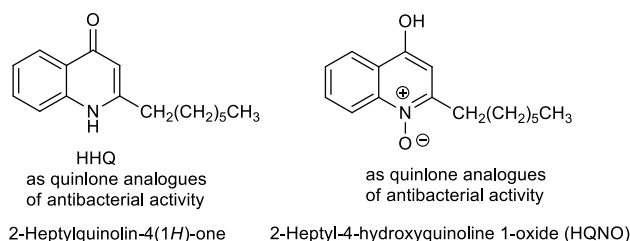
3,3′-arylmethylene-bis-(4-hydroxyquinolin-2(1*H*)-ones. Aly et al. [19] also reported another method of preparing arylmethylene-bis-3,3′-quinoline-2-ones via the reaction of equal equivalents of aromatic amines and diethyl malonate together with half equivalent of the corresponding aromatic aldehydes. 3,3′-Arylmethylene-bis(4-hydroxyquinolin-2(1*H*)-ones have a great biological activity especially in the composition of vitamin K [22, 23] and anticoagulation [24]. Choudhary et al. [25] synthesized some 3,3′-methylenebis(substituted-4-hydroxyquinolin-2(1*H*)-ones from the condensation between two molecules of quinolones and one molecule formaldehyde but also neither mechanism nor NMR spectra were discussed for the products. Previously, irradiation of only *N*-ethyl(methyl)-4-hydroxyquinol-2-ones, was tested in ethanol and afforded their corresponding 3,3′-methylenebis(substituted-4-hydroxyquinolin-2(1*H*)-ones, virtually eliminating the solvent as a source of formaldehyde [26]. The method suffered from low yields of the obtained products besides to its hazard condition. Moreover the stereochemistry of the obtained products was not discussed.

Utilizing by the expected formylation process during the reaction of 2-quinolones with dimethylformamide/triethylamine (DMF/Et$_3$N) mixture [27, 28], we explain the abnormal formation of 3,3′-methylenebis(4-hydroxyquinolin-2(1*H*)-ones. Also, the previous two aforementioned methods could not afford a general preparation method and suffered from low yields, hazardous conditions and no spectroscopic detailed data compared to our announced method of preparation.

Coronavirus disease (COVID-19) is a respiratory infectious disease caused by a novel virus strain, severe acute respiratory syndrome-coronavirus 2 (SARS-CoV-2) [29–32]. Molecular docking is utilized as a substantial tool in the drug discovery process to predict the binding mode and affinity of a drug candidate with a target. To combat COVID-19, the main protease of SARS-CoV-2 (M^{pro}) would be targeted due to its significant role in the viral replication

Fig. 1 DMF as a precursor of various functional groups

Fig. 2 The structures of 2-heptylquinolin-4(1*H*)-one (HHQ) and 2-heptyl-4-hydroxyquinoline 1-oxide (HQNO) as alkyl-quinolone (AQ) analogues

process. Therefore, the binding modes and affinities of 3,3′-methylenebis(4-hydroxyquinolin-2(1H)-ones) as prospective SARS-CoV-2 inhibitors were predicted against M^{pro} using Darunavir as a drug reference. Darunavir (DrugBank code: DB01264) is a human immunodeficiency virus (HIV) protease inhibitor and has been recently clinical investigated as anti-COVID-19 drug [33, 34]. The aforementioned encouraged us to synthesize various derivatives of 3,3′-methylenebis(4-hydroxyquinolin-2(1H)-ones) and established a general method of preparing the former compounds. In addition, we investigate the molecular docking of 3,3′-methylenebis(4-hydroxyquinolin-2(1H)-ones) as anti-COVID-19 using Darunavir as a prospective drug reference.

Results and discussion

Upon addition of equimolar amounts of 4-hydroxy-2(1H)-quinolones **1a–g** and Et$_3$N and gently heating in an oil path at 70–80 °C using DMF for 10–12 h, the resulting yellowish orange coloration of the solution was converted gradually to brown color and the 3,3′-methylenebis(substituted-4-hydroxyquinolin-2(1H)-ones **3a–g** were precipitated in 70–87% yields (Scheme 1).
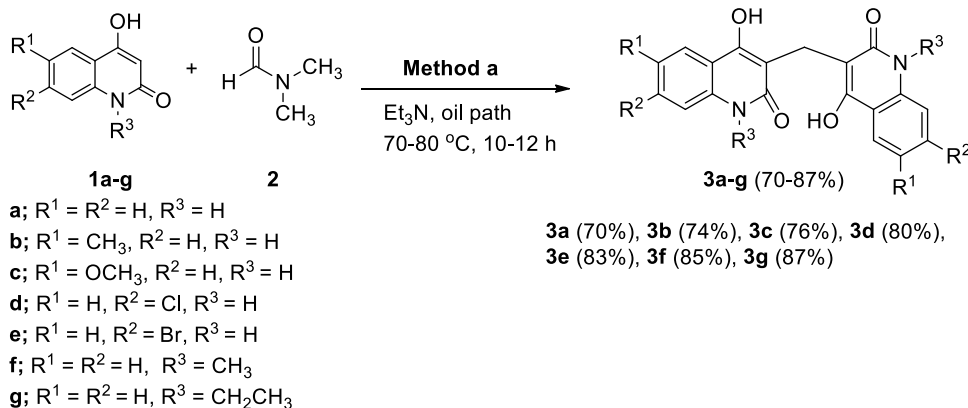
The structural assignment of all the obtained products **3a–g** were based on IR, NMR (^{1}H NMR and ^{13}C NMR,) and mass spectra were performed; these and elemental analyses were in good agreement with the assigned structures. As an example, 3,3′-methylene-bis(1-ethyl-4-hydroxyquinolin-2(1H)-one (**3g**). The elemental analysis and mass spectrometry of compound **3g** have the gross formula C$_{23}$H$_{22}$N$_2$O$_4$. The IR spectrum of **3g** indicated the presence of OH at $\nu = 3500$ (OH), 3030 (Ar–CH), 2867 (Alpihatic –CH) and 1643 cm^{-1} (C=O), whereas CH$_2$ group at $\nu = 1458$ cm^{-1}. The ^{1}H NMR spectrum of **3g** exhibited a triplet at $\delta_H = 1.24$ and a quartet at 4.38 ppm with the coupling constant $J = 7.50$ Hz arising from ethyl group. The ^{1}H NMR spectrum of **3g** also showed the methylene protons at $\delta_H = 3.89$. Eight aromatic protons give rise to characteristic signals in the aromatic region of

the spectrum, whereas the hydroxyl protons resonated at $\delta_H = 12.65$. The presence of methylene (CH$_2$) group is evident from ^{13}C-DEPT-NMR spectra; exhibiting positive signal at $\delta_H = 12.95$ ppm and negative signal at $\delta_H = 37.59$ ppm (CH$_2$). The ^{13}C NMR spectrum of **3g** showed signals at $\delta_C = 131.50$, 122.67, 123.30 and 116.74 ppm due to Ar–CH (C-7), (CH-6), (CH-5) and (CH-8), respectively (Fig. 3). The ^{13}C NMR spectrum of **3g** supported the ^{13}C NMR spectroscopic data by the distinctive appearance of carbon signals representing quinolone C-4a and C-8a (Fig. 3) and resonated at $\delta_C = 115.15$ and 136.70 ppm, respectively. Also, the observed δ_C values for carbon atoms in C-2 at $\delta_C = 164.84$, C-4 at 159.63 and C-3 at 108.53 ppm.
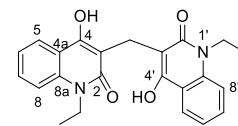
The structure of **3g** was unambiguously determined by a single crystal structure determination showing the bismethylene system (Fig. 4 and see CIF file, note that the crystallographic numbering does not correspond to the systematic IUPAC numbering rules). The bond lengths C(3)–C(21) and C(13)–C(21) are 1.5085 (15) Å and 1.5104 (14) Å, respectively, and have single bond character, while C=O of 1.2536 (13) Å and 1.2605 (13) Å, has double bond character. Whereas, bond lengths C(3)–C(4) 1.3637 (15) Å, C2–C3 1.4384 (15) Å and N1–C2 1.3796 (14) Å indicate the presence of hydrogen bond between O2–H14–O14 and O12-H4-O4.

The *anti*-form of the formed compound is established and stabilized by the formed hydrogen bonding. On the basis of the previous reports [1, 27], the formation of 3,3′-methylenebis(substituted-4-hydroxyquinolin-2(1H)-ones **3a–g** can be rationalized as depicted in Scheme 2. It would be proposed that Et$_3$N would abstract a hydrogen proton from the active methylene in C-3 of **1a–g** and therefore increasing the nucleophilicty of CH-3 of the quinolone

Fig. 3 Structure and numbering of compound **3g**

Scheme 1 Formation of 3,3′-methylenebis(substituted-4-hydroxyquinolin-2(1H)-ones from the reaction of 4-hydroxy-2-quinolones **1a–g** with DMF **2** and Et$_3$N

1a–g　　　**2**
a; R^1 = R^2 = H, R^3 = H
b; R^1 = CH$_3$, R^2 = H, R^3 = H
c; R^1 = OCH$_3$, R^2 = H, R^3 = H
d; R^1 = H, R^2 = Cl, R^3 = H
e; R^1 = H, R^2 = Br, R^3 = H
f; R^1 = R^2 = H, R^3 = CH$_3$
g; R^1 = R^2 = H, R^3 = CH$_2$CH$_3$

3a–g (70–87%)

3a (70%), **3b** (74%), **3c** (76%), **3d** (80%), **3e** (83%), **3f** (85%), **3g** (87%)
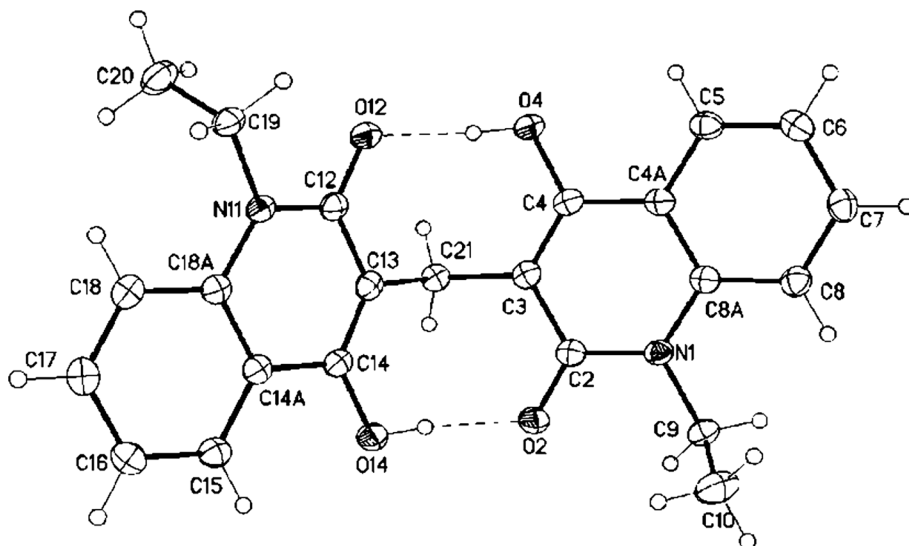
moiety. Thereafter, a nucleophilic addition of the anion CH-3 of **1a–g** to the carbonyl carbon of DMF would give the intermediate **4** accompanied by elimination of a molecule of dimethylamine, $(CH_3)_2NH$ to give 4-formyl-2-quinolones (**5**). Reaction of **5** with **2** via the nucleophilic attack of the oxygen lone pair to the carbonyl in **2** would form intermediate **6** (Scheme 2). Subsequently, elimination of another molecule of dimethylamine $(CH_3)_2NH$ would give the intermediate **7**. Further nucleophilic attack of a molecule of **1** to vinylic-carbon in **7** would form the intermediate **8**. Finally, decarboxylation of **8** would form compound **3** (Scheme 3). The reaction pathway was also supported via isolation of $(CH_3)_2NH$, which was identified by TLC analysis.

Having established reaction conditions in hand, we investigated the formation **3a–g** from the reaction of 3-formyl-4-hydroxy-2-quinolone derivatives **5a–g** with **1a–g** under the condition illustrated in Scheme 3. We reacted **5a–g** with their resemble derivatives in **1a–g** to obtain symmetric compounds like those in Scheme 1. Fortunately, the target symmetric products of 3,3′-methylenebis(substituted-4-hydroxyquinolin-2(1H)-ones) **3a–g** were formed in 60–77% yields (Scheme 3).

Molecular docking calculations

Utilizing molecular docking technique, the binding modes and affinities of compounds **3a–g** as prospective SARS-CoV-2 inhibitors were predicted against the main protease (M^{pro}). The geometrical structures of **3a–g** were prepared and docked into the active site of SARS-CoV-2 M^{pro} using AutoDock 4.2.6 software with docking parameters of GA = 250 and eval = 25,000,000. The predicted binding scores and features are summarized in Table 1. The 2D representations of binding modes of the investigated compounds inside the active site of SARS-CoV-2 M^{pro} are depicted in Fig. 5.
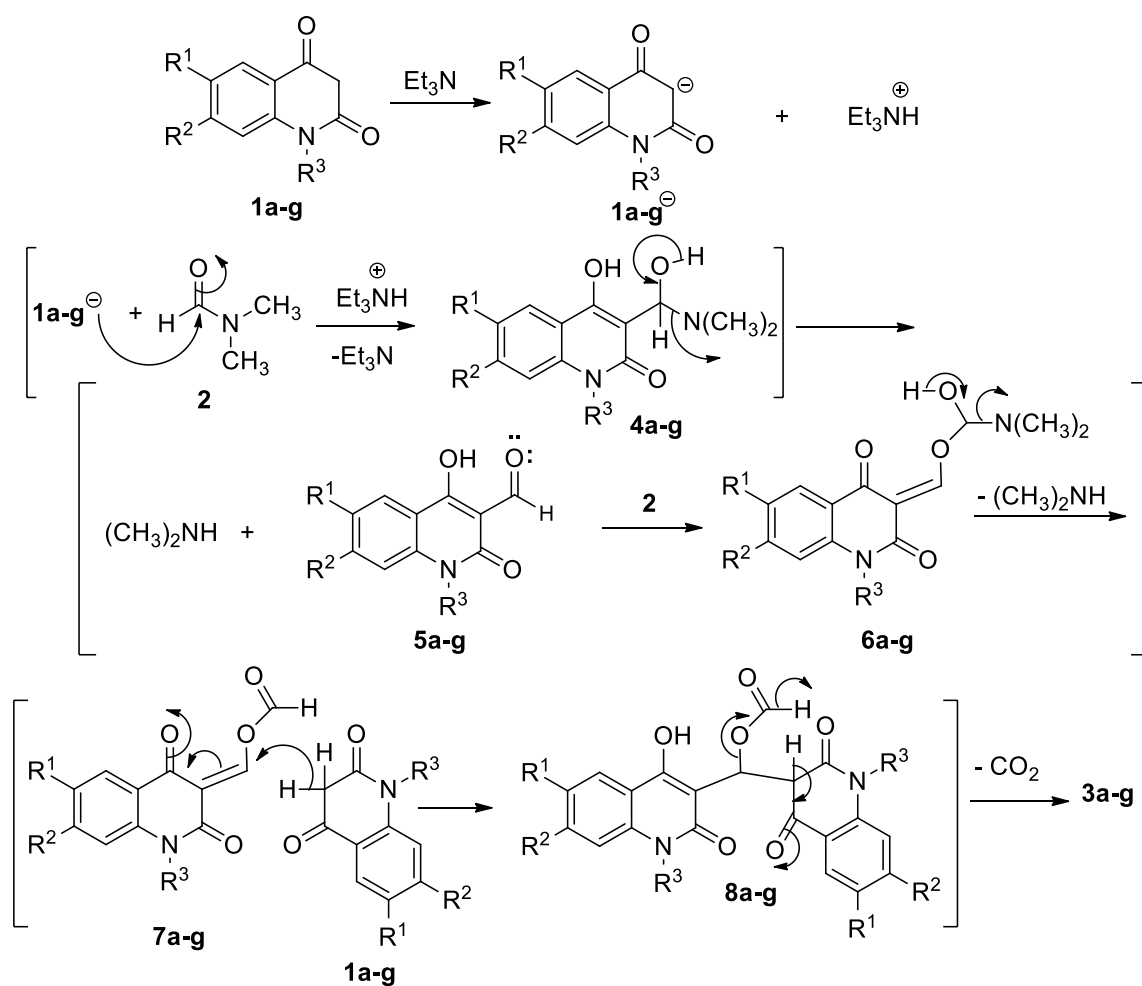
What is interesting about the data in Table 1 is that compounds **3a–g** demonstrated good binding affinities toward SARS-CoV-2 M^{pro} with docking scores ranged from −8.63 to −7.05 kcal/mol. Besides, compounds **3a–g** exhibited the same binding modes inside the active site of M^{pro}, forming an essential hydrogen bond with key amino acid GLU166 residue (Fig. 5). Further interactions including van der Waals, hydrophobic and pi-based interactions were also observed between the compound and the key amino acids inside the SARS-CoV-2 M^{pro} active site (Fig. 5).

Among the examined compounds, **3e** showed the highest binding affinity with docking score of −8.6 kcal/mol against SARS-CoV-2 M^{pro}. The high potentiality of **3e** as SARS-CoV-2 M^{pro} inhibitor would be returned to its capability to form four hydrogen bonds with THR190, GLN192, ARG188 and GLU166 amino acid with bond lengths of 2.10, 2.38, 1.79 and 2.08 Å, respectively (Figs. 5, 6).
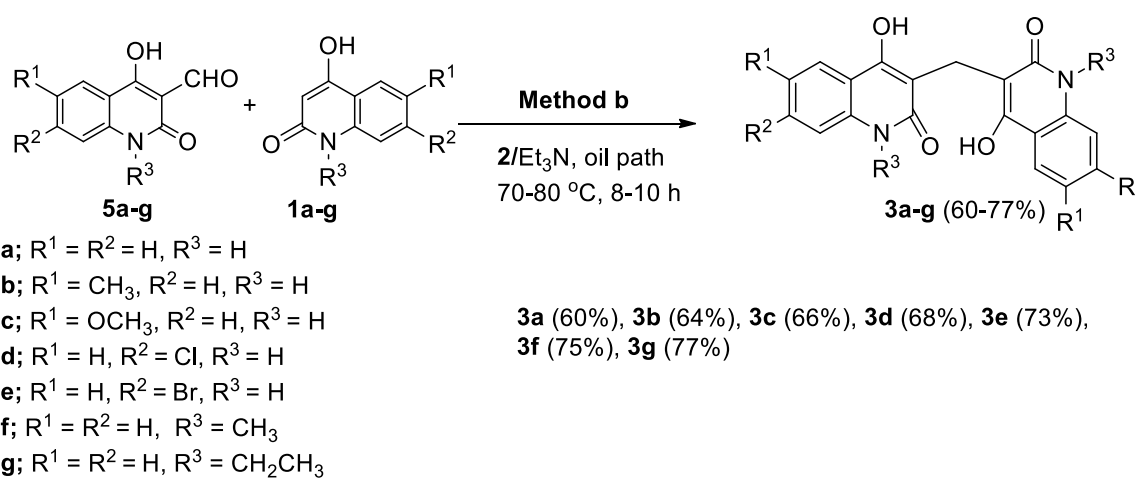
The binding affinity and features of Darunavir were investigated and compared to compound **3e** as SARS-CoV-2 M^{pro} inhibitors. According to molecular docking calculations, Darunavir showed a good binding affinity of −8.19 kcal/mol, forming three hydrogen bonds with GLU166, and LEU167 with bond lengths of 1.94, 2.88 and 1.96 Å, respectively (Figs. 5, 6). A comparison of the molecular docking results revealed the competing binding affinity of **3e** with regard to Darunavir as prospective SARS-CoV-2 M^{pro} inhibitor.

Conclusion

Formylation of 2-quinolones by DMF/Et₃N mixture caused an insertion of a methylene group between two symmetrically quinolones. DMF/Et₃N mixture was proved as a formylatig agent of the parent 2-quinolones. Reaction of 4-formyl-2-quinolone with the parent 2-quinolone under the

Fig. 4 X-ray structure analysis of **3g** (displacement parameters drawn at 50% probability level)

Scheme 2 The proposed mechanism describes the formation of compounds **3a–g**

a; $R^1 = R^2 = H$, $R^3 = H$
b; $R^1 = CH_3$, $R^2 = H$, $R^3 = H$
c; $R^1 = OCH_3$, $R^2 = H$, $R^3 = H$
d; $R^1 = H$, $R^2 = Cl$, $R^3 = H$
e; $R^1 = H$, $R^2 = Br$, $R^3 = H$
f; $R^1 = R^2 = H$, $R^3 = CH_3$
g; $R^1 = R^2 = H$, $R^3 = CH_2CH_3$

3a (60%), **3b** (64%), **3c** (66%), **3d** (68%), **3e** (73%),
3f (75%), **3g** (77%)

Scheme 3 Formation of compounds **3a–g** from the reaction of 3-formyl-4-hydroxy-2-quinolones **5a–g** with **1**, **2** and Et$_3$N

Table 1 Molecular docking scores and binding features for compound **3a–g** and Darunavir with SARS-CoV-2 main protease (M^{pro})

No.	Compound	Docking score (kcal/mol)	Binding features (hydrogen bond length in Å
1	**3a**	−8.28	ARG188 (2.18 Å), MET165 (2.63 Å), HIS164 (2.14 Å), GLU166 (2.17 Å, 2.79 Å)
2	**3b**	−8.14	ARG188 (2.81 Å), GLN192 (2.37 Å), THR190 (2.09 Å), GLU166 (2.03 Å)
3	**3c**	−7.05	ARG188 (1.82 Å), THR190 (2.60 Å) GLN192 (1.93 Å), GLU166 (1.82 Å, 1.96 Å)
4	**3d**	−8.30	GLU166 (2.05 Å), ARG 188 (1.80 Å), THR190 (2.08 Å), GLN192 (2.38 Å)
5	**3e**	−8.63	THR190 (2.1 Å), GLN192 (2.38 Å), ARG188 (1.79 Å), GLU166 (2.08 Å)
6	**3f**	−7.72	GLN189 (1.94 Å), GLU166 (2.01 Å, 2.33 Å)
7	**3g**	−7.38	GLU166 (2.82 Å)
8	Darunavir	−8.19	GLU166 (1.94 Å, 2.88 Å), LEU167 (1.96 Å)

same reaction condition gave the same product. The aforesaid 3-formyl-2-quinolones would prospectively be used to prepare various symm and/or asymm substitutents of the desired compounds. Molecular docking calculations demonstrated the competing binding affinity of **3e** with regard to Darunavir as a prospective SARS-CoV-2 M^{pro} inhibitor.

Experimental

The IR spectra were recorded by ATR technique (ATR = Attenuated Total Reflection) with a FT device (FT-IR Bruker IFS 88), Institute of Organic Chemistry, Karlsruhe University, Karlsruhe, Germany. The NMR spectra were measured in DMSO-d_6 on a Bruker AV-400 spectrometer, 400 MHz for ^{1}H, and 100 MHz for ^{13}C; and the chemical shifts are expressed in δ (ppm), versus internal tetramethylsilane (TMS) = 0 for ^{1}H and ^{13}C, and external liquid ammonia = 0. The description of signals includes: s = singlet, d = doublet, t = triplet, q = quartet, m = multiplet, dd = doublet of doublet and m = multiplet. Mass spectra were recorded on a FAB (fast atom bombardment) Thermo Finnigan Mat 95 (70 eV). Elemental analyses were carried out at the Microanalytical Center, Cairo University, Egypt. TLC was performed on analytical Merck 9385 silica aluminum sheets (Kieselgel 60) with Pf$_{254}$ indicator; TLC's were viewed at λ_{max} = 254 nm.

Starting materials

1,6-Disubstituted-quinoline-2,4-(1*H*,3*H*)-diones **1a–g** were prepared according to the literature [35, 36] whereas carbaldehydes **5a**, **5b**, **5c–f** and **5g** were synthesized according to the literature [37–40].

General procedure

Method a: A mixture of **1a–g** (1 mmol), 15 ml of DMF (**2**), 0.100 g (1 mmol) Et$_3$N was gently heated with stirring in

an oil path at 70–80 °C for 10–12 h. The time period until the reactants had disappeared, as mentioned in Scheme 1, was monitored by TLC. The formed precipitate was then washed with ethanol (50 mL) and recrystallized from the stated solvents to give pure crystals of **3a–g**. The filtrate was concentrated on vacuum and (CH$_3$)$_2$NH was obtained and was identified by TLC analysis.

Method b: A a mixture of **1a–g** (1 mmol), **5a–g** (1 mmol) and 0.100 g (1 mmol) of Et$_3$N in **2** 15 ml of **2** was gently heated with stirring for 8–10 h in an oil path at 70–80 °C. Compounds **3a–g** were obtained (i.e., Scheme 3) in pure state as above mentioned.

3,3′-Methylenebis(4-hydroxyquinolin-2(1*H*)-one) (**3a**). Orange crystals (DMF/H$_2$O), yield (**method a**): 0.233 g (70%) or yield (**method b**) 0.200 g (60%); ^{1}H NMR (400 MHz, DMSO-d_6): δ = 3.59 ppm (s, 2H, CH$_2$), 7.05–7.07 (m, 2H, Ar–H), 7.17–7.19 (m, 2H, Ar–H), 7.30–7.35 (m, 2H, Ar–H), 7.65–7.71 (m, 2H, Ar–H), 11.99 (s, 2H, NH), 12.54 ppm (s, 2H, OH); ^{13}C NMR (100 MHz, DMSO-d_6): δ = 19.16 (CH$_2$), 109.12 (C-3), 115.85 (C-4a), 115.96 (C-8), 122.52 (C-6), 122.78 (C-5), 130.87 (C-7), 136.80 (C-8a), 160.77 (C-4), 165.94 ppm (C-2); MS (Fab, 70 eV, %): m/z = 334 (M$^+$, 15), 227 (15), 136 (62), 120 (23), 107 (27), 89 (15). *Anal*. Calcd. for C$_{19}$H$_{14}$N$_2$O$_4$ (334.33): C, 68.26; H, 4.22; N, 8.38. *Found*: C, 68.38; H, 4.35; N, 8.42.

3,3′-Methylenebis(4-hydroxy-6-methylquinolin-2(1*H*)-one) (**3b**) [25]. Orange crystals (DMF/EtOH), yield (**method a**): 0.267 g (74%) or yield (**method b**): 0.231 g (64%); ^{1}H NMR (400 MHz, DMSO-d_6): δ = 2.25 (s, 6H, CH$_3$), 3.78 (s, 2H, CH$_2$), 7.20–7.29 (m, 2H, Ar–H), 7.30–7.40 (m, 2H, Ar–H), 7.65–7.71 (m, 2H, Ar–H), 12.21 (s, 2H, NH), 12.78 ppm (s, 2H, OH); ^{13}C NMR (100 MHz, DMSO-d_6): δ = 19.23 (CH$_2$), 20.59 (CH$_3$), 109.12 (C-3), 115.77 (C-4a), 115.88 (C-8), 122.14 (C-5), 131.66 (C-7), 132.15 (C-6), 134.82 (C-8a), 160.62 (C-4), 165.71 ppm (C-2); MS (Fab, 70 eV, %): m/z = 362 (M$^+$, 25), 226 (25), 136 (63), 120 (22), 107 (28), 89 (13). *Anal*. Calcd. for C$_{21}$H$_{18}$N$_2$O$_4$ (362.38): C, 69.60; H, 5.01; N, 7.73. *Found*: C, 69.74; H, 4.89; N, 7.83.
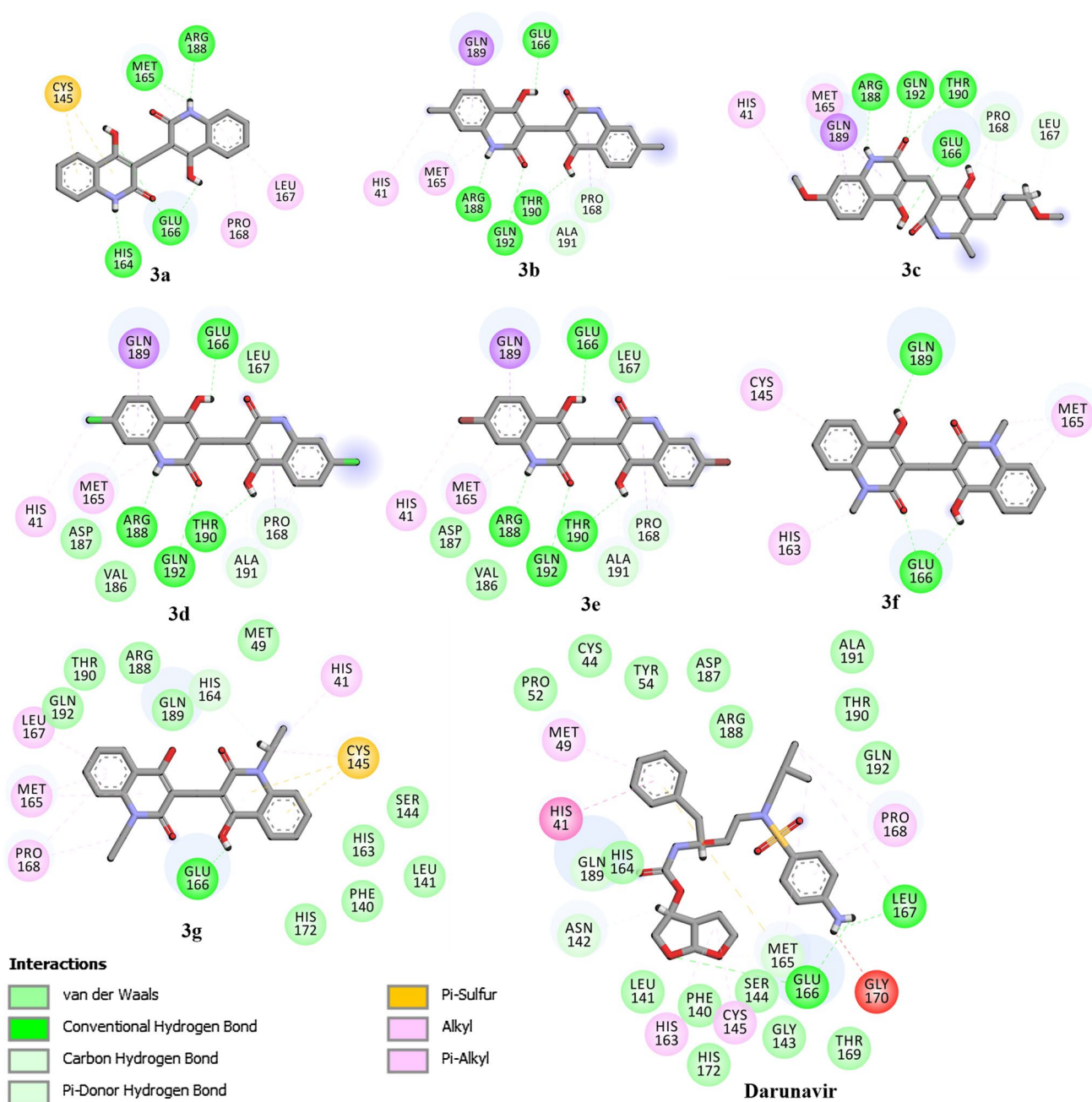
Fig. 5 2D representation of predicted binding mode of **3a–g** inside the active site of COVID-19 main protease (M^pro^)

3,3′-Methylenebis(4-hydroxy-6-methoxyquinolin-2(1*H*)-one) (**3c**). Orange crystals (DMF/CH₃OH), yield (**method a**): 0.230 g (76%) or yield (**method b**): 0.260 g (66%); mp = 330–332 °C; IR (KBr): ν = 3450 (OH), 2910 (NH), 3008 (Ar–CH), 1660 (CO), 1453 cm⁻¹ (CH₂); ¹H NMR (400 MHz, DMSO-d_6): δ = 3.81 (s, 6H, OCH₃), 3.78 (s, 2H, CH₂), 7.24–7.30 (m, 2H, Ar–H), 7.32–7.38 (m, 2H, Ar–H), 7.60–7.72 (m, 2H, Ar–H), 12.13 (s, 2H, NH), 12.96 ppm (s, 2H, OH); ¹³C NMR (100 MHz, DMSO-d_6): δ = 19.23 (CH₂), 55.37 (OCH₃), 109.11 (C-3), 115.76 (C-4a), 115.87

(C-8), 122.13 (C-5), 131.62 (C-7), 132.13 (C-6), 134.82 (C-8a), 160.61 (C-4), 165.69 ppm (C-2); MS (Fab, 70 eV, %): *m/z* = 394 (M⁺, 20), 136 (63), 120 (9), 107 (18), 89 (13). *Anal. Calcd. for* C₂₁H₁₈N₂O₆ (394.38): C, 63.96; H, 4.60; N, 7.10. *Found*: C, 63.84; H, 4.72; N, 7.19.

3,3′-Methylenebis(7-chloro-4-hydroxyquinolin-2(1*H*)-one) (**3d**) [25]. Orange crystals (DMF/CH₃OH), yield (**method a**): 0.322 g (80%) or yield (**method b**): 0.274 g (68%); ¹H NMR (400 MHz, DMSO-d_6): δ = 3.78 (s, 2H, CH₂); 7.22–7.28 (m, 2H, Ar–H), 7.30–7.39 (m, 2H, Ar–H),

Fig. 6 3D representations of interactions of **3e** and Darunavir with important amino acid residues of COVID-19 main protease (M^{pro})

3e   Darunavir
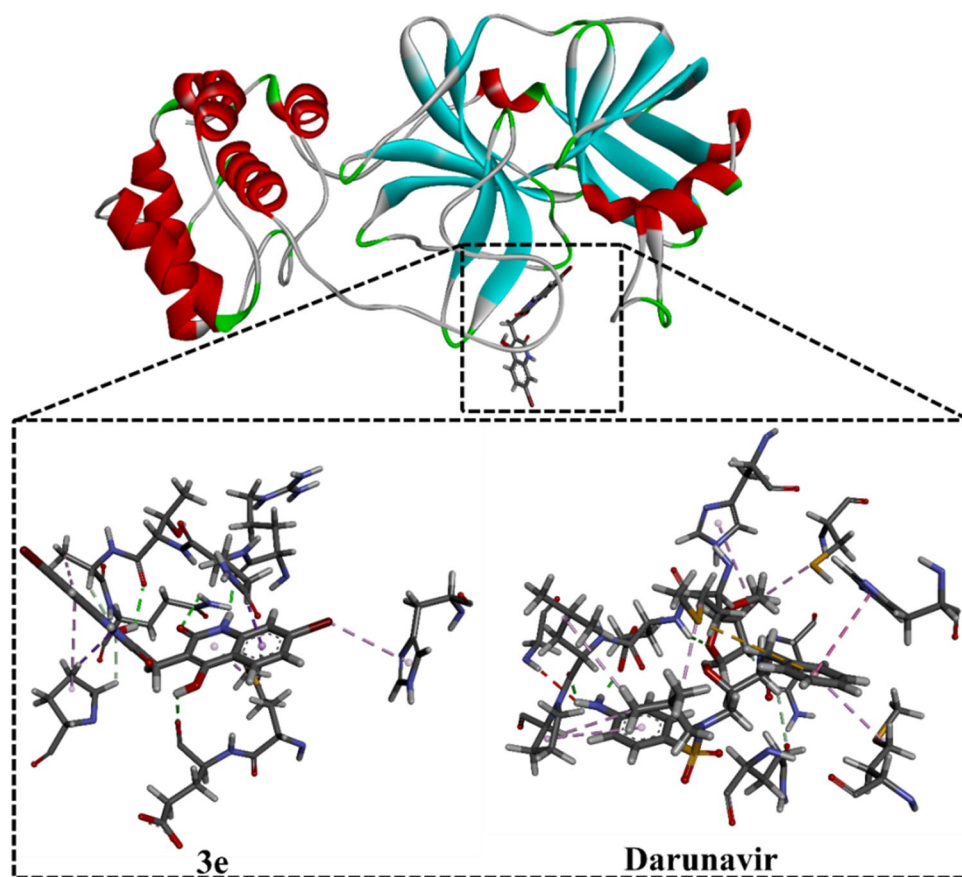
7.62–7.70 (m, 2H, Ar–H), 12.15 (s, 2H, NH), 12.86 ppm (s, 2H, OH); ^{13}C NMR (100 MHz, DMSO-d_6): $\delta = 20.01$ (CH$_2$), 109.00 (C-3), 115.70 (C-4a), 115.02 (C-8), 122.13 (C-6), 130.00 (C-5), 132.13 (C-7), 136.82 (C-8a), 160.62 (C-4), 164.69 ppm (C-2); MS (Fab, 70 eV, %): $m/z = 403/402$ (/20/18), 136 (63), 120 (9), 107 (18), 89 (13). *Anal. Calcd. for* C$_{19}$H$_{12}$Cl$_2$N$_2$O$_4$ (402.02): C, 56.60; H, 3.00; N, 6.95. *Found*: C, 56.49; H, 3.12; N, 7.14.

3,3′-Methylenebis(7-bromo-4-hydroxyquinolin-2(1*H*)-one) (**3e**) [25]. Orange crystals (DMF/EtOH), yield (**method a**): 0.406 g (83%) or yield (**method b**): 0.357 g (73%); ^{1}H NMR (400 MHz, DMSO-d_6): $\delta = 3.77$ (s, 2H, CH$_2$), 7.22–7.25 (m, 2H, Ar–H), 7.26–7.30 (m, 2H, Ar–H), 7.70–7.82 (m, 2H, Ar–H), 12.14 (s, 2H, NH), 12.90 ppm (s, 2H, OH); ^{13}C NMR (100 MHz, DMSO-d_6): $\delta = 19.80$ (CH$_2$), 109.10 (C-3), 115.76 (C-4a), 115.10 (C-8), 122.10 (C-6), 128.90 (C-5), 132.98 (C-7), 136.82 (C-8a), 160.58 (C-4), 165.12 ppm (C-2); MS (Fab, 70 eV, %): $m/z = 490/489$ (20/18), 136 (63), 120 (10), 107 (20), 89 (10). *Anal. Calcd. for* C$_{19}$H$_{12}$Br$_2$N$_2$O$_4$ (489.12): C, 46.37; H, 2.46; N, 5.69. *Found*: C, 46.48; H, 2.36; 5, 7.73.

3,3′-Methylenebis(4-hydroxy-1-methylquinolin-2(1*H*)-one) (**3f**) [26]. Orange crystals (DMF/EtOH), yield (**method a**): 0.308 g (85%) or yield (**method b**): 0.272 g (75%); IR (KBr): $\nu = 3450$ (OH), 3040 (Ar–CH), 2820 (CH-Aliphatic),

1641 (CO), 1417 cm^{-1} (CH$_2$); ^{1}H NMR (400 MHz, DMSO-d_6): $\delta = 3.72$ (s, 6H, CH$_3$), 3.60 (s, 2H, CH$_2$), 7.10–7.14 (m, 2H, Ar–H), 7.25–7.31 (m, 4H, Ar–H), 7.72–7.78 (m, 2H, Ar–H), 12.87 ppm (s, 2H, OH); ^{13}C NMR (100 MHz, DMSO-d_6): $\delta = 19.15$ (CH$_2$), 38.01 (CH$_3$), 109.13 (C-3), 115.80 (C-4a), 115.97 (C-8), 122.53 (C-6), 122.77 (C-5), 130.98 (C-7), 136.82 (C-8a), 160.66 (C-4), 165.80 ppm (C-2); MS (Fab, 70 eV, %): $m/z = 362$ (M$^+$, 33), 136 (63), 120 (10), 107 (20), 89 (10). *Anal. Calcd. for* C$_{21}$H$_{18}$N$_2$O$_4$ (362.38): C, 69.60; H, 5.01; N, 7.73. *Found*: C, 69.72; H, 5.12; N, 7.65.

3,3′-Methylenebis(1-ethyl-4-hydroxyquinolin-2(1*H*)-one) (**3g**) [26]. Orange crystals (DMF/EtOH), yield (**method a**): g 0.340 (87%) or yield (**method b**): 0.300 g (77%); IR (KBr): $\nu = 3500$ (OH), 3030 (Ar–CH), 2867 (CH-Aliphatic), 1643 (CO), 1458 cm^{-1} (CH$_2$); ^{1}H NMR (400 MHz, DMSO-d_6): $\delta = 1.24$ (t, 6H, CH$_3$), 3.89 (s, 2H, CH$_2$), 4.38 (q, 4H, CH$_2$), 7.00–7.05 (m, 2H, Ar–H), 7.29–7.35 (m, 2H, Ar–H), 7.59–7.70 (m, 4H, Ar–H), 7.90–8.07 (m, 2H, Ar–H), 12.65 ppm (s, 2H, OH); ^{13}C NMR (100 MHz, DMSO-d_6): $\delta = 12.95$ (CH$_2$-Et), 21.11 (CH$_2$), 37.59 (CH$_3$-Et), 108.52 (C-3), 115.15 (C-4a), 116.74 (C-8), 122.67 (C-6), 123.30 (C-5), 131.50 (C-7), 136.70 (C-8a), 159.63 (C-4), 164.83 ppm (C-2); MS (Fab, 70 eV, %): $m/z = 390$ (M$^+$, 18), 202 (12), 136 (62), 120 (12), 107 (20), 89 (20). *Anal. Calcd.*

for $C_{23}H_{22}N_2O_4$ (390.42): C, 70.75; H, 5.68; N, 7.17. *Found*: C, 70.82; H, 5.77; N, 7.29.

Crystal structure determination

The single-crystal X-ray diffraction study of **3g** was carried out on a Bruker D8 Venture diffractometer with Photon II detector at 123(2) K using Cu-Kα radiation ($\lambda = 1.54178$ Å). Dual space/intrinsic methods (SHELXT) [41] were used for structure solution and refinement was carried out using SHELXL-2014 (full-matrix least-squares on F^2) [42]. Hydrogen atoms were localized by difference electron density determination and refined using a riding model (H(O) free). A semi-empirical absorption correction was applied.

3g: Orange crystals, $C_{23}H_{22}N_2O_4$, $M_r = 390.42$, crystal size $0.36 \times 0.24 \times 0.12$ mm, monoclinic, space group $P2_1/c$ (No. 14), $a = 13.2293$ (3) Å, $b = 17.0327$ (4) Å, $c = 8.5503$ (2) Å, $\beta = 101.919$ (1)°, $V = 1885.11$ (8) Å^3, $Z = 4$, $\rho = 1.376$ Mg/m^{-3}, $\mu(\text{Cu-K}_\alpha) = 0.77$ mm^{-1}, $F(000) = 824$, $2\theta_{max} = 144.4°$, 16886 reflections, of which 3689 were independent ($R_{int} = 0.024$), 268 parameters, 2 restraints, $R_1 = 0.034$ (for 3587 $I > 2\sigma(I)$), w$R_2 = 0.089$ (all data), $S = 1.06$, largest diff. peak/hole $= 0.27/-0.19$ e Å^{-3}.

Molecular docking calculations

All molecular docking calculations were carried out using Autodock 4.2.6 software [43]. The crystal structure of SARS-CoV-2 main protease (M^{pro}; PDB code: 6LU7 [44]) was taken as a template for all molecular docking calculations. Water molecules, ions and the ligand were deleted. The protonation state of M^{pro} was evaluated using H^{++} server, and all missing hydrogen atoms were added [45]. All docking parameters were kept to default values, except the number of genetic algorithm (GA) run and the maximum number of energy evaluation (eval) which were set to 250 and 25,000,000, respectively. The docking grid was set to 60 Å × 60 Å × 60 Å with a grid spacing value of 0.375 Å, and the grid center was placed at the center of the active site of M^{pro}. The geometrical structures of all examined synthesized compounds were minimized with MMFF94s force field using SZYBKI software [46] and the partial atomic charges were assigned using Gasteiger method [47].

Supporting Information

CCDC 2011538 (**3g**) contains the supplementary crystallographic data for this paper. These data can be obtained free of charge from The Cambridge Crystallographic Data Centre via www.ccdc.cam.ac.uk/data_request/cif.

References

1. Muzart J (2009) N, N-Dimethylformamide: much more than a solvent. Tetrahedron 65:8313–8323. https://doi.org/10.1016/j.tet.2009.06.091

2. Wu Y, Seyedsayamdost MR (2017) Synergy and target promiscuity drive structural divergence in bacterial alkylquinolone biosynthesis. Cell Chem Biol 24:1437–1444. https://doi.org/10.1016/j.chembiol.2017.08.024

3. Burden DA, Osheroff N (1998) Mechanism of action of eukaryotic topoisomerase II and drugs targeted to the enzyme. Biochim Biophys Acta 1400:139–154. https://doi.org/10.1016/S0167-4781(98)00132-8

4. Chin YW, Salim AA, Su BN, Mi Q, Chai HB, Riswan S, Kardono LBS, Ruskandi A, Farnsworth NR, Swanson SM, Kinghorn AS (2008) Potential anticancer activity of naturally occurring and semisynthetic derivatives of aculeatins A and B from *Amomum aculeatum*. J Nat Prod 71:390–395. https://doi.org/10.1021/np070584j

5. Obniska J, Kamiński K (2006) Synthesis and anticonvulsant properties of new *N*-phenylamino derivatives of 2-azaspiro[4.4]nonane, 2-azaspiro[4.5]decane-1,3-dione and 3-cyclohexylpyrrolidine-2,5-dione Part IV. Acta Polon Pharm 63(2):101–108

6. Kamiński K, Obniska J, Dybała M (2007) Synthesis, physicochemical and anticonvulsant properties of new N-phenylamino derivatives of 2-azaspiro[4.4]nonane- and [4.5]decane-1,3-diones: part V. Eur J Med Chem 43(1):53–61. https://doi.org/10.1016/j.ejmech.2007.02.024

7. Obniska J, Kamiński K, Tatarcyńska E (2006) Impact of aromatic substitution on the anticonvulsant activity of new *N*-(4-arylpiperazin-1-yl)-alkyl-2-azaspiro[4,5]decane-1,3-dione derivatives. Pharmacol Rep 58:207–214

8. Nakao K, Ikeda K, Kurokawa T, Togashi Y, Umeuchi H, Honda T, Okano K, Mochizuki H (2008) Effect of TRK-820, a selective κ opioid receptor agonist, on scratching behavior in an animal model of atopic dermatitis. Nihon Shinkei Seishin Yakurigaku Zasshi (Jpn J Psychopharmacol) 28:75–83

9. Park HB, Jo NH, Hong JH, Chei JH, Cho JH, Yoo KH, Oh CH (2007) Synthesis and in vitro activity of novel 1β-methylcarbapenems having Spiro[2,4]heptanes moieties. Arch Pharm Chem Life Sci (Weinheim) 340(10):530–537. https://doi.org/10.1002/ardp.200700060

10. Pawar MJ, Burungale AB, Karale BK (2009) Synthesis and antimicrobial activity of spiro[chromeno[4,3-*d*][1,2,3]thiadiazole-4,1'-cyclohexane, spiro[chromeno[4,3-*d*][1,2,3]selenadiazole-4,1'-cyclohexane and spiro [chroman-2,1'-cyclohexan]-4-one-5-spiro-4-acetyl-2-(acetyl-amino)-Δ2-1,3,4-thiadiazolines compounds. Arkivoc 13:97–107. https://doi.org/10.3998/ark.5550190.0010.d08

11. Fujio M, Hashimoto K, Katayama J, Numata A, to Welfide Corp (2001) Preparation of spiro[azabicycloalkane-oxazolidinone] derivatives and analogs as α-7 nicotinic receptor agonists 066546. PCT Int Appl WO Chem Abstr 135:318499

12. Schick H, Frank R, Reich M, Jostock R, Bahrenberg G, Theil F, Henkel B, to Gruenenthal GmbH (2006) Preparation of 1-oxa-2,8-diazaspiro[4.5]dec-2-enes as vanilloid receptor 1 inhibitors122769. PCT Int Appl WO Chem Abtrs 145:505458

13. Hu H, Guo H, Li E, Liu X, Zhou Y, Che Y (2006) Decaspirones F − I, bioactive secondary metabolites from the saprophytic fungus *Helicoma viridis*. J Nat Prod 69:1672–1675. https://doi.org/10.1021/np0603830

14. Sarma BK, Manna D, Minoura M, Mugesh G (2010) Synthesis, structure, spirocyclization mechanism, and glutathione peroxidase-like antioxidant activity of stable spirodiazaselenurane and spirodiazatellurane. J Am Chem Soc 132:5364–5374. https://doi.org/10.1021/ja908080u

15. Plaska E, Aytemir M, Uzbay ÌT, Erol D (2001) Synthesis and antidepressant activities of some 3,5-diphenyl-2-pyrazolines. Eur J Med Chem 36:539–543. https://doi.org/10.1016/S02235234-(01)01243-0

16. Aly AA, El-Sheref EM, Mourad A-FE, Brown AB, Bräse S, Bakheet MEM, Nieger M (2018) Synthesis of spiro(indoline-3,4'-pyrano[3,2-c]quinoline)-3'-carbonitriles. Monatshefte für Chem 149:635–644. https://doi.org/10.1007/s00706-017-2078-6

17. Aly AA, Ishak EA, Shawky AM, Mohamed AH (2020) Formation of furo[3,2-c]quinolone-2-carbonitriles and 4-oxo-4,5-dihydrofuro[3,2-c]quinolone-2-carboxamides from reaction of quinoline-2,4-diones with 2-[bis(methylthio)-methylene] malononitrile. Monatshefte für Chem 151:223–229. https://doi.org/10.1007/s00706-019-02541-0

18. Aly AA, El-Sheref EM, Bakheet MEM, Mourad MAE, Bräse S, Ibrahim MAA, Nieger M, Garvalov BK, Dalby KN, Kaoud TS (2019) Design, synthesis and biological evaluation of fused naphthofuro[3,2-*c*]quinoline-6,7,12-triones and pyrano[3,2-*c*]quinolone-6,7,8,13-tetraones derivatives as ERK inhibitors with efficacy in BRAF-mutant melanoma. Bioorg Chem 82:290–305. https://doi.org/10.1016/j.bioorg.2018.10.044

19. Aly AA, El-Sheref EM, Mourad A-FE, Bräse S, Bakheet MEM, Nieger M (2019) One-pot synthesis of 2,3-bis-(4-hydroxy-2-oxo-1,2-dihydroquinolin-3-yl)succinates and aryl methylene-bis-3,3'-quinoline-2-ones. Chem Pap 73:27–37. https://doi.org/10.1007/s11696-018-0561-0

20. Aly AA, El-Sheref EM, Bakheet MEM, Mourad A-FE, Brown AB, Bräse S, Nieger M (2018) Synthesis of novel 1,2-bis-quinolinyl-1,4-naphthoquinones: ERK2 inhibition, cytotoxicity and molecular docking studies. Bioorg Chem 81:700–712. https://doi.org/10.1016/j.bioorg.2018.09.017

21. Han L, Zhou Z (2019) An efficient and green protocol for synthesis of 3,3'-arylmethylene-bis(4-hydroxyquinolin-2(1H)-ones) using potassium phthalimide as reusable Catalyst. J Mater Environ Sci 10(2):182–186

22. Mentzer C, Meunier P, Lecocq J, Billet D, Xuong D (1945) Chemical studies of the antivitamin K series of compounds. Bull Soc Chim Fr 12:430–437

23. Meunier P, Mentzer C, Buu-Hoi Cagniant P (1943) Antivitamins K. II. Formation of a naphthalene derivative with hemorrhagic activity. Bull Soc Chim Biol Paris 25:384–390

24. Fucik K, Prochazka Z, Hach V, Strof J (1951) Anticoagulant substances. VIII. Nitrogen analogs of dicoumarol and pelentan. Chem Listy Pro Vedu a Prumysl 45:23–25

25. Choudhary CD, Das RR, Choudhary S (2008) Study of dimerization reactions of 4-hydroxycarbostyril/substituted 4-hydroxy carbostyril. Orient J Chem 24(1):259–260

26. Hunt RG, Potter CJ, Reid ST, Roantree ML (1975) The photoaddition of 4-hydroxycoumarin and *N*-methyl-4-hydroxyquinol-2-one to cyclohexene. Tetrahedron Lett 28:2327–2330. https://doi.org/10.1016/0040-4039(75)80002-5

27. Kumar R, Wadhwa D, Prakash O (2010) Beckmann rearrangement of 2-hydroxy-5-methylacetophenone oxime using Vilsmeier-Haack reagent (POCl$_3$/DMF): synthesis of some new heterocycles. Heterocycl Commun 16:201–205. https://doi.org/10.1515/HC.2010.16.2-3.201

28. Koeller S, Lellouche JP (1999) Preparation of formate esters from *O*-TBDMS/*O*-TES protected alcohols. A one-step conversion using the Vilsmeier-Haack complex. Tetrahedron Lett 40:7043–7046. https://doi.org/10.1016/S0040-4039(99)01453-7

29. Boopathi S, Poma AB, Kolandaivel P (2020) Novel 2019 coronavirus structure, mechanism of action, antiviral drug promises and rule out against its treatment. J Biomol Struct Dyn. https://doi.org/10.1080/07391102.2020.1758788

30. Seah I, Agarwal R (2020) Can the coronavirus disease 2019 (COVID-19) affect the eyes? A review of coronaviruses and ocular implications in humans and animals. Ocul Immunol Inflamm 28(3):391–395. https://doi.org/10.1080/09273948.2020.1738501

31. Gupta MK, Vemula S, Donde R, Gouda G, Behera L, Vadde R (2020) In-silico approaches to detect inhibitors of the human severe acute respiratory syndrome coronavirus envelope protein ion channel. J Biomol Struct Dyn. https://doi.org/10.1080/07391102.2020.1751300

32. Yuan M, Yin W, Tao Z, Tan W, Hu Y (2020) Association of radiologic findings with mortality of patients infected with 2019 novel coronavirus in Wuhan, China. PLoS ONE 15(3):e0230548. https://doi.org/10.1371/journal.pone.0230548

33. Meyer SD, Bojkova D, Cinati J, Damme EV, Buyck C, Loock MV, Woodfall B, Ciesek S (2020) Lack of antiviral activity of darunavir against SARS-CoV-2. Int J Infect Dis 5:85–91. https://doi.org/10.1101/2020.04.03.20052548

34. McKee DL, Sternberg A, Stange U, Laufer S, Naujokat C (2020) Candidate drugs against SARS-CoV-2 and COVID-19. Pharmacol Res 157:104859. https://doi.org/10.1016/j.phrs.-2020.104859

35. Rao VS, Darbarwar M (1988) One pot synthesis of 7-[1,2-dihydro-4-hydroxy-1-methyl/phenyl-2-oxo-3-quinolinyl]-5,7-dihydro-5-methyl/phenyl-6*H*-[1]-benzo-pyrano-[3,2-*c*]quinolin-6-ones. Synth Commun 18:2267–2272. https://doi.org/10.1080/00397918808082369

36. Buckle DR, Cantello BCC, Smith H, Spicer BA (1975) 4-Hydroxy-3-nitro-2-quinolones and related compounds as inhibitors of allergic reactions. J Med Chem 18:726–732. https://doi.org/10.1021/jm00241a017

37. Bhudevi B, Ramana PV, Mudiraj A, Reddy AR (2009) Synthesis of 4-hydroxy-3-formylideneamino-l*H*/methyl/phenylquinolin-2-ones. Indian J Chem B 48:255–260

38. Mohamed EA, Ismail MM, Gaber Y, Abass M (1994) Synthesis of some multiazaheterocycles as substituents to quinolone moiety of specific biologicalactivity. Chem Pap 48:285–292

39. Aly AA, Mohamed AH, Ramadan M (2020) Synthesis and colon anticancer activity of some novel thiazole/-2-quinolone derivatives. J Mol Struct 1207:127798. https://doi.org/10.1016/j.molstruc.2020.127798

40. Jayashree A, Darbarwar M (2010) Synthesis of 3-amino-4,5-dihydro(5*H*)4-oxothieno[3,2-*c*]quinoline-2-carboxylic acids and their alkyl ester. J Indian Chem Soc 87:325–330. https://doi.org/10.1002/chin.201101140

41. Sheldrick GM (2015) SHELXT—integrated space-group and crystal-structure determination. Acta Crystallogr A 71:3–8. https://doi.org/10.1107/S2053273314026370

42. Sheldrick GM (2015) Crystal structure refinement with SHELXL. Acta Crystallogr C71:3–8. https://doi.org/10.1107/S2053229614024218

43. Morris GM, Huey R, Lindstrom W, Sanner MF, Belew RK, Goodsell DS, Olson AJ (2009) AutoDock4 and AutoDockTools4: automated docking with selective receptor flexibility. J Comput Chem 30(16):2785–2791. https://doi.org/10.1002/jcc.21256

44. Jin Z, Du X, Xu Y, Deng Y, Liu M, Zhao Y, Zhang B, Li X, Zhang L, Peng C, Duan Y, Yu J, Wang L, Yang K, Liu F, Jiang R, Yang

X, You T, Liu X, Yang X, Bai F, Liu H, Liu X, Guddat LW, Xu W, Xiao G, Qin C, Shi Z, Jiang H, Rao Z, Yang H (2020) Structure of M^pro from COVID-19 virus and discovery of its inhibitors. Nature 582:289–293. https://doi.org/10.1038/s41586-020-2223-y

45. Gordon JC, Myers JB, Folta T, Shoja V, Heath LS, Onufriev A (2005) H++: a server for estimating pKas and adding missing hydrogens to macromolecules. Nucl Acids Res 33:W368–W371. https://doi.org/10.1093/nar/gki464

46. SZYBKI OpenEye Scientific Software, Santa Fe, NM, USA

47. Gasteiger J, Marsili M (1980) Iterative partial equalization of orbital electronegativity—a rapid access to atomic charges. Tetrahedron 36(22):3219–3228. https://doi.org/10.1016/0040-4020(80)80168-2

Affiliations

Ashraf A. Aly[1] · **Alaa A. Hassan[1]** · **Asmaa H. Mohamed[1]** · **Esraa M. Osman[1]** · **Stefan Bräse[2,3]** · **Martin Nieger[4]** · **Mahmoud A. A. Ibrahim[1]** · **Sara M. Mostafa[1]**

✉ Ashraf A. Aly
ashrafaly63@yahoo.com; ashraf.shehata@mu.edu.eg

[1] Department of Chemistry, Faculty of Science, Minia University, Minia 61519, Egypt

[2] Institute of Organic Chemistry, Karlsruhe Institute of Technology, 76131 Karlsruhe, Germany

[3] Institute of Biological and Chemical Systems (IBCS-FMS), Karlsruhe Institute of Technology, Eggenstein-Leopoldshafen, Germany

[4] Department of Chemistry, University of Helsinki, A. I. Virtasenaukio I, P.O. Box 55, 00014 Helsinki, Finland